Nano Res (2009) 2: 660–670
DOI 10.1007/s12274-009-9069-9
Research Article

CO Dissociation and CO+O Reactions on a Nanosized Iron Cluster

Giorgio Lanzani[1], Albert G. Nasibulin[2], Kari Laasonen[1] (✉), and Esko I. Kauppinen[2] (✉)

[1] Department of Chemistry, P.O. Box 3000, FIN-90014 University of Oulu, Finland
[2] Department of Applied Physics and Center for New Materials, Helsinki University of Technology, P.O. Box 5100, FIN-02150 Espoo, Finland

Received: 9 April 2009 / Revised: 24 May 2009 / Accepted: 8 June 2009

ABSTRACT

Catalysis over metal nanoparticles is essential for the growth of carbon nanotubes and all the properties of the resulting nanotube, such as diameter and chirality, are affected by the metal particle. Thus, it is very important to understand the carbon chemistry taking place on nanometer size metal particles. Here we present the first ab initio computational study of chemical reactions on a nanosized iron cluster. The clusters have reaction sites, such as edges and vertexes between the facets, Which have not been studied before. First principles electronic structure calculations, fully incorporating the effects of spin polarization and non-collinear magnetic moments, have been used to investigate CO disproportionation on an isolated Fe_{55} cluster. After CO dissociation, O atoms remain on the surface while C atoms move into the cluster, presumably as the initial step toward carbide formation. Here we show that the lowest CO dissociation barrier found on the cluster (0.77 eV) is lower than on most previously studied Fe surfaces. This dissociation occurs on a vertex between the facets. Several possible paths for CO_2 formation were identified. The calculated lowest reaction barrier is 1.08 eV, which is comparable to the barrier of 0.65 eV obtained by experiment.

KEYWORDS

Nanoparticle, density functional theory (DFT), mechanism, synthesis

Since their discovery, carbon nanotubes (CNTs) have been the object of very intensive research. CNTs are of great interest since they exhibit unique and useful chemical and physical properties related to toughness, electrical/thermal conductivity, and magnetism [1]. Several different techniques have been introduced to synthesize CNTs [2–5] but among the various routes, carbon vapor deposition (CVD) methods have attracted widespread interest since they open a way to highly controlled and continuous CNT production on designed architectures [5–9]. In these processes, metal nanoparticles are produced in a mixed flow of carbon precursors and other gases (e.g., hydrogen) and the growth process is driven by cleaving the carbon atoms from the precursors and these atoms then form carbon structures on the surface of the nanoparticles. The metal catalyst nanoparticle is essential for CNT growth. All properties, like diameter and chirality, of the nanotube are determined by the metal particle. The ability to control the properties of CNTs is essential for their use in technological applications [10]. Thus, it

Address correspondence regarding the computational part to Kari Laasonen, Kari.Laasonen@oulu.fi; address correspondence regarding the CVD part to Esko I. Kauppinen, Esko.Kauppinen@hut.fi

is very important to understand the carbon chemistry taking place on the nanometer size metal particles.

In addition to the CNT synthesis, metal nanoclusters with a size less than 10 nm have attracted a great deal of attention due to their applications in magnetism [11], electronics [12], and catalysis [13]. Often the good catalytic activity can be related to catalytic sites, like atomic size steps, on the cluster. Due to the high curvature of the clusters, the special site density and distribution are much higher than on almost all other surfaces. Furthermore, real nanoclusters have several unique active sites like facets and vertexes between the facets which can have catalytic properties that differ drastically from the ones on almost all other surfaces. For example, gold, which is rather inert as a bulk metal, has high reactivity in the form of nanosized clusters; the origin of their catalytic properties is still widely debated, however [14–16]. Research related to active sites is mainly limited to atomic steps on surfaces, and nanosized clusters have received much less attention [17–20]. If we want to understand the active sites on clusters, we have to know which cluster we are studying. Even then each cluster has several different active sites, and it is very difficult to know which of them is the most active. For this reason the computational approach, where precise sites can be studied, is very attractive.

Carbon monoxide (CO) is one of the most common carbon sources for the production of CNTs [9, 21–23]. This is due to the reasonable temperature range for CO disproportionation and the good CNT yield. Also the thermal self-decomposition of CO, leading to the precipitation of amorphous carbon and the formation of soot particles, can be avoided. The essential role of etching agents (CO_2 and H_2O) in CNT formation in the CVD process has been demonstrated [24]. These molecules are assumed to etch the amorphous carbon that can poison the catalyst particles needed for CO disproportionation, as well as for the CNT nucleation and growth. The important role of H_2 in the CVD process has also been shown [31]. The H_2 is believed to prevent the oxidation of the nanosized catalyst iron particles. Another possible role is in a reaction with CO_2: $CO_2+2H_2\rightarrow 2H_2O+C$, which can provide additional carbon for the CNT synthesis. An earlier work has attempted to explain the effect of hydrogen in carbon fiber formation [27]. They suggested that the role of H_2 is to limit or alleviate the carbon poisoning of the metal catalysts. More recently, it has been proposed that an intermediate, known as precursor soot, is involved in the formation of multi-walled carbon nanotubes (MWCNTs) and that H_2 reduces the rate of dehydrogenation of the CH_x intermediates which form the soot [28].

To understand the chemistry of CNT formation on a catalytic particle several reactions need to be considered. In the ideal case, with only CO as precursor, these include the dissociation of CO, CO_2 formation and release of C, the migration of carbon into the bulk of the catalyst, segregation of carbon to the surface, and the formation of graphene networks. These reactions are already quite complex and any additional new atom will make the reactions much more complex and thus a complete study with three species, like C, O, and H, is probably an unreachable goal with present computational resources. For these reasons, this study addresses the disproportionation of isolated CO molecules on iron nanoclusters ($CO_{(g)}+CO_{(g)}\leftrightarrow CO_{2(g)}+C_{(s)}$) and the dissociation of H_2. The detailed chemistry on the surface of CNT catalyst transition metal nanoparticles is largely unknown, but it is believed that the adsorbed CO first dissociates, $CO_{(ads)}\rightarrow C_{(ads)}+O_{(ads)}$, and then $O_{(ads)}$ reacts with an undissociated $CO_{(ads)}$ to form surface $CO_{2(ads)}$ (Fig. 1) [25, 26].

In order to understand the role of the cluster in this reaction, we have used first principles calculations to study the steps of this reaction on a small nanocluster. To our knowledge, there have been few ab initio studies of nanosized clusters [29, 30] and these works do not address any chemical

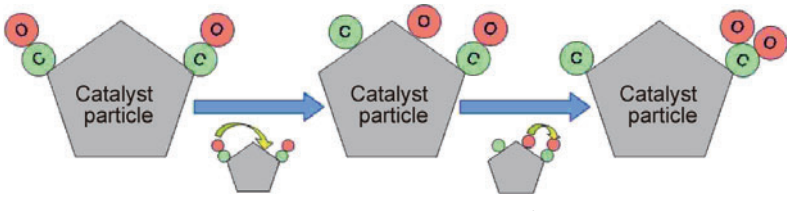

Figure 1 Proposed CO disproportionation mechanism (Fe, grey; C, green; and O, red)

reactions. The nanoparticles have features that cannot be studied on stepped surfaces, and this work will complement existing studies of such active sites. The computational work is combined with experimental investigations of the same reaction on larger nanoclusters [31, 32].

1. Methods

The method for the production of single-walled carbon nanotubes (SWCNTs) has been described in detail elsewhere [31, 32]. In this method, pre-made catalyst particles of controlled size, concentration, and polydispersity are introduced under well defined synthesis conditions. Briefly, catalyst particles were produced from Fe vaporized from a resistively heated catalyst wire in a H_2/N_2 (with a 7/93 molar ratio) flow (400 cm^3/min). Particles were formed and grown by vapor nucleation, condensation, and particle collision processes. Subsequently, the resulting particles were introduced into either a ceramic or stainless steel tubular reactor, mixed with a CO flow (400 cm^3/min) and heated to induce CNT formation. Reactor wall peak temperatures ranged from 890 °C to 1207 °C.

For electronic structure calculations, we have used density functional theory (DFT) with gradient correction and plane wave basis set within the super-cell approach (VASP code [33]). The adequacy of the functional form, pseudopotentials and plane wave basis set has been tested against the calculation of cluster geometry. Iron has a large magnetic moment and in the cluster geometry, the spin orientation is determined by subtle effects. Therefore, we have fully incorporated the effects of spin polarization and non-collinear magnetic moments in our calculations [34]. To our knowledge this is the first time that these effects have been included when substrate molecules or reactivity on nanoclusters is considered. Preliminary test calculations of the magnetic and structural properties of iron clusters up to Fe_{55} has been performed using $E_{Cut\text{-}off}$ up to 270 eV with cubic super cell with size between 17 Å and 30 Å. This cluster is the best choice for our study because it is the largest one that we have been able to simulate whilst obtaining good results for the magnetic and geometric properties [34]. Good results were obtained with a super-cell size of 21 Å, with $E_{Cut\text{-}off}$=250 eV. These settings are also used for the rest of calculations. The cluster has an icosahedral geometry and has a formation energy of –3.87 eV/atom. The largest Fe–Fe distance was 9.68 Å. The dipole moment was (–0.05; –0.03; 0.04) el Å; and the magnetic moment was (2.33; 0.48; 1.06) μB/atom. The reactions barriers are more demanding to study and special transition state search algorithms, like climbing-image nudged elastic band (CI-NEB) [39], have been used for their determination. According to this algorithm, a set of 3*N*-dimensional images of the adsorbate system are generated between the endpoint configurations. A harmonic interaction between adjacent images is added to ensure continuity of the path, thus mimicking an elastic band. An optimization of the band, involving the minimization of the forces acting on the images, brings the band to the minimum energy path.

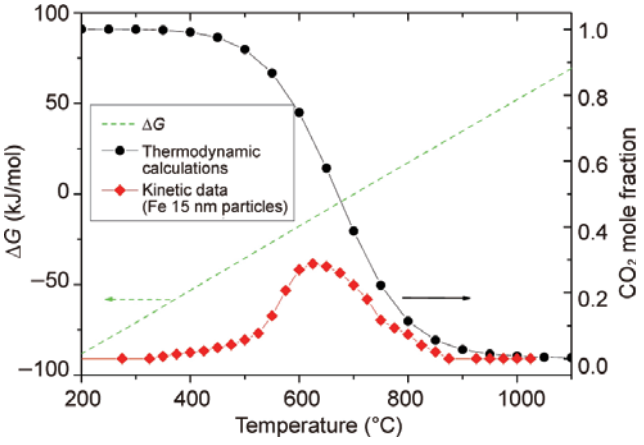

Figure 2 Temperature dependence of the Gibbs free energy for the CO disproportionation reaction. The equilibrium concentration of CO_2 and kinetic data for CO disproportionation on the surface of 15 nm sized iron particles as a function of temperature are also plotted in the figure

2. Results

A gas-phase process for formation of SWCNTs, based on thermal decomposition of iron pentacarbonyl or ferrocene in the presence of carbon monoxide (CO), was investigated in ambient pressure laminar flow reactors in the temperature range 600–1300 °C [31]. *In situ* sampling carried out at 1000 °C showed that the growth of SWCNTs occurred from individual

metal particles in the heating section of the furnace in the temperature range 891–928 °C, during which the growth rate was estimated to exceed 2 μm/s [32]. Kinetic investigations of the CO disproportionation reaction were performed in a horizontal quartz tube at a heating rate of 5 °C/min from room temperature. A silica substrate with deposited 15 nm sized iron particles was placed inside the tube. The CO flow rate through the tube was maintained at 8.3 cm^3/min. The concentration of the gaseous product (CO_2) was monitored on-line by infrared (IR). Investigations using 15 nm sized iron particles show appreciable reaction rates in the temperature interval from 470 to 820 °C with a maximum rate at about 625 °C (Fig. 2). The region of CO_2 concentration increase from about 325 °C to about 600 °C is the kinetic region, where the rate of the CO disproportionation reaction can be measured. At temperatures above 625 °C, this reaction is limited thermodynamically as can be seen from the values of Gibbs free energy, ΔG. Since the disproportionation reaction rate is proportional to the concentration of CO_2, the activation energy of the reaction can be found using an Arrhenius dependence: $X_{CO_2}=k_0 \exp(-E_a/RT)$, where X_{CO_2} is the carbon dioxide mole fraction. Plotting the kinetic region in the coordinates of $\ln X_{CO_2}$ versus $1/T$, one gets $k_0=7.16091$ and $E_a=63031$ J/mol=0.65 eV as an energy barrier for the CO disproportionation reaction (Fig. 3).

Theoretical calculations (VASP code [33]) have been used to study the geometry of a 1 nm size Fe_{55} cluster and to identify the stationary points of the species involved in the reactions on it. In order to understand the reaction mechanism, several reaction paths have been studied. Our results suggest that the energetically most favorable cluster has an icosahedral symmetry. In this conformation, the 55-atom cluster has three atomic layers, one atom in the center, a 12-atom inner icosahedron, and a 42-atom outer icosahedron. Our results are in good agreement with the density functional based study of Kohler et al. [34]. The geometries and bonding energies of the adsorbates (CO, CO_2, H_2, and atomic C/O) were calculated using the same computation approach used for the icosahedral Fe_{55}. The geometry optimization was started from the high symmetry adsorption sites on one of the cluster faces. The high symmetry adsorption sites are the top site (T_S), the octahedral hollow site (H_S), and the bridge sites (B_S). The T_S and B_S sites exist both on the cluster faces and on its edges/Vertexes. H_S sites are on the triangular faces of the icosahedral Fe_{55}: *A* and *E* in plane hexagonal close packed (hcp) site (Fig 4). B_S sites are located in on the facet (plane bridge site) like *B* (Fig 4); or on the edge bridge site (*C* in Fig 4); T_S site are vertex top sites, *D* and *F*, on edge top site (Fig. 4). The adsorption energy (E_{ads}) is defined as $E_{ads}=E_{Fe_{55}+mol}-(E_{Fe_{55}}+E_{mol})$, where $E_{Fe_{55}+mol}$ is the total energy of the cluster with adsorbates, E_{Fe55} is the total energy of the

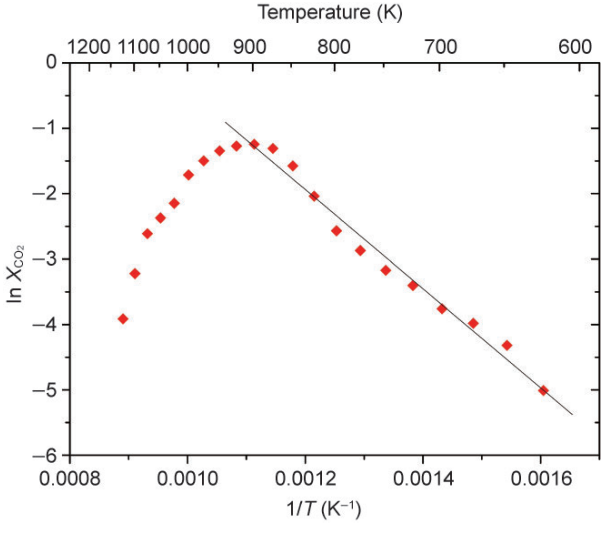

Figure 3 Kinetic region of the CO disproportionation reaction fitted with a straight line (Arrhenius plot)

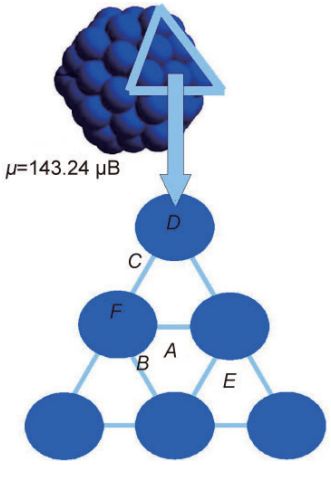

Figure 4 High symmetry adsorption sites on a triangular face of the icosahedral Fe_{55}: *A*, in plane hexagonal close packed (hcp) site; *B*, in plane bridge site; *C*, on edge bridge site; *D*, on vertex top site; *E*, in plane hcp site; and *F*, on edge top site

Fe_{55} cluster, and E_{mol} is the total energy of free ½ O_2, ½ H_2, CO, CO_2 molecules or C atom. Thus, the more negative is E_{ads}, the stronger is the adsorption.

For CO, geometries with both the molecular bond coplanar (=) or perpendicular (p) to the cluster surface were considered. The total magnetic moment of each structure is reported in the figures and tables. Only the perpendicular adsorption with the molecule adsorbed through the carbon is stable. During the optimization, CO spontaneously moved to the edge of the face (*D* and *F* sites in Fig. 4). The most favored adsorption site for CO is the T_S site on the vertex of the cluster (*F* in Fig. 4) having E_{ads}=–1.83 eV, followed by the *D* site with 0.40 eV higher energy. On the cluster *F* and *D* sites, the C–O bond is elongated to 1.181 Å and 1.179 Å, respectively (cf. 1.144 Å for free CO). These results can be compared with the reported binding energies and stable geometries for CO on different Fe surfaces at low coverage (θ =0.25). For the stepped Fe (211) surface, DFT calculations by Borthwick et al. [46] propose the p-CO interaction on the step of the surface as the most stable geometry (E_{ads}=–1.73 eV, and C–O bond length 1.17 Å). This is in good agreement with the lowest values, –1.81 eV and –1.43 eV, reported here. DFT calculations of Chen et al. [35] gave E_{ads}=–1.65 eV for the p-CO adsorption on the T_S site of the Fe (111) surface. A similar on-top adsorption geometry has also been obtained on the less open Fe (110) and Fe (100) surfaces [36, 45] with respective adsorption energies of –2.00 eV and –1.392 eV. These results suggest that at low coverage, the CO adsorption on the Fe_{55} cluster is comparable to previously studied Fe surfaces.

A systematic study of the stability of CO_2 on the vertex and edge of the cluster was considered as well as on the planar faces, through a series of geometry optimizations starting from several different molecular orientations. Among these possible initial geometries, only four stable conformations were found and the CO_2 geometry was distorted. The adsorption energies (–0.39 eV<*E*<–0.11 eV) and corresponding geometries are reported in Fig. 5. The minimum energy configuration (E_{ads}=–0.39 eV) corresponds to the bridge site with one of the molecular bonds lying on the cluster surface (labeled as CO_2_*B*1 in Fig. 5). In this configuration, the CO_2 molecule is bent

Adsorbate	Adsorption site		E_{ads} (eV)	μ (μB)	Geometry
CO_2 (molecule)	*B*	CO_2_*B*1	–0.39	143.68	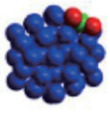
		CO_2_*B*2	–0.29	143.61	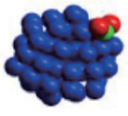
	F	CO_2_*F*1	–0.24	143.39	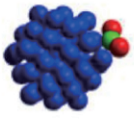
		CO_2_*F*2	–0.11	143.53	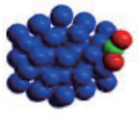

Figure 5 Stable geometries of CO_2 on Fe_{55} (Fe, blue; C, green; and O, red)

(molecular angle=152°), with the carbon–oxygen bond closer to the surface at a distance of 1.90 Å and elongated to 1.36 Å (cf. 1.16 Å for the free molecule). The other C–O bond has a length of 1.31 Å. Adsorption is also possible on *F* sites. In this case, the molecule has C_{2v} symmetry and the molecular plane is upright to the cluster and parallel or perpendicular to the edge direction. These latter cases are local minimum configurations corresponding to weaker bonding, with E_{ads}=–0.24 eV. In this configuration (labeled as CO_2_*F*1 in Fig. 5), the CO_2 molecule is bent, with the carbon atom closer to the surface at about 1.92 Å and the C–O bond lengths are equal to 1.28 Å. The adsorption of CO_2 on various transition metals has been the subject of many investigations. The geometries we obtained are in accordance with the results suggested in the previous literature [37].

In order to study CO dissociation and CO_2 formation with the (CI-NEB) method [38, 39], we need to investigate the preferred C and O coadsorption on the cluster. First, all possible adsorption sites were considered, and only three stable sites for individually adsorbed C and O were

located. Both of the atoms show the same behavior (Fig. 6): H_S or T_S are the only stable sites and from the bridge sites, the adsorbate migrates to the nearest hollow site. Table 1 displays the adsorption energies of isolated C or O atoms on the high-symmetry sites; for comparisons remember that the reference energy for carbon is the isolated atom, and that for the oxygen is half of the O_2 molecule. We found that the H_S sites (E in Fig. 6) are the most favorable ones with E_{ads} (O) = –4.27 eV and E_{ads} (C) = –7.96 eV. The observed Fe_3C structures, corresponding to carbon adsorption on the H_S sites, were also previously observed on different Fe surfaces [40–42].

Table 1 Binding energies for the main adsorption geometries of H_2, atomic oxygen and atomic carbon on Fe_{55}

Adsorption site	Binding energy (eV)		
	H_2	O	C
A	+0.09	–3.87	–7.91
B	–0.36	–4.23	–7.99
C	+0.28	–4.26	–7.98
D	–0.03	–2.96	–5.83
E	+0.26	–4.27	–7.96
F	–0.03	–4.23	–6.44

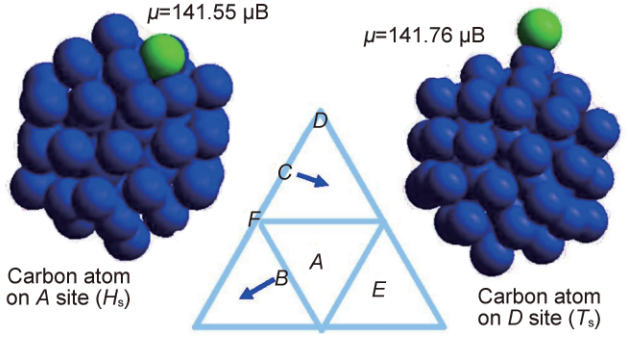

Figure 6 Schematic representation of the stable geometries of atomic carbon on Fe_{55}. Atomic oxygen shows similar behavior. (Fe, blue; and C, green)

Next, we placed both C and O atoms near each other on the same face of the cluster. All the possible coadsorption combinations were considered, but only six geometries (reported in Fig. 7) have exothermic dissociative chemisorption (ΔE), defined as $\Delta E = (E_{Fe_{55}/C+O} - (E_{Fe_{55}} + E_{CO}))/N_{CO}$, where $E_{Fe_{55}/C+O}$ is the total energy of the cluster with atomic C/O co-adsorbates and N_{CO} is the number of free CO molecules. Interestingly, it seems that having an O atom nearby pushes the C atom onto another face of the cluster. We also found that for the most stable geometries (indicated as C_O_2 and C_O_3 in Fig. 7), the O atom remains on the surface while the C atom is embedded into cluster, indicating C atoms may indeed diffuse into the bulk. This carbide-like behavior was suggested in the previous literature [43]. This behavior is also in line with previous Raman ellipsometry spectroscopy observation [49] of surfaces. In these studies, Watanabe et al. found that CO dissociation produces a thin Fe_3O_4 layer on Fe surfaces, which blocks a large number of C atoms in the metallic phase.

Adsorbate	Adsorption site		ΔE (eV)	μ (μB)	Geometry
C (atom) + O (atom) on the same face	C_O_1	O on *A* site / C on *E* site	–0.32	141.01	
	C_O_2	O on *E* site / C on *C* site	–2.44	141.06	
C (atom) + O (atom) on different face	C_O_3	O on *A* site / C on *A* site	–2.50	141.03	
	C_O_4	O on *E* site / C on *E* site	–1.97	141.77	
	C_O_5	O on *E* site / C on *E* site	–1.78	141.40	
	C_O_6	O on *E* site / C on *E* site	–0.99	141.90	

Figure 7 Stable geometries of C + O on Fe_{55} showing exothermic dissociative chemisorption (Fe, blue; C, green; and O, red)

The stability of H_2 on the cluster was also considered. The resulting binding energies for H_2 adsorption perpendicular to the cluster surface are reported in Table 1. During the geometry optimization starting from the top sites, the molecule keeps its position in a metastable state, but from the other sites H_2 spontaneously dissociates and one

adsorbate migrates below the surface. Schematic representation of the main adsorption geometries is reported in Fig. 8. In this work we will not study further the reactions of hydrogen and other species, but the atomic hydrogen will react very easily with O, C, and larger C clusters.

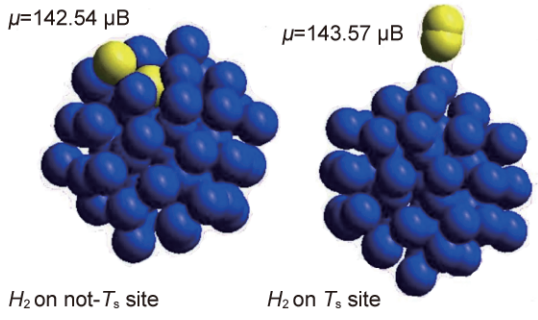

Figure 8 The main adsorption geometries of H_2 on Fe_{55} (Fe, blue; and H, yellow)

Based on CO adsorption and C/O co-adsorption data, CO dissociation paths from the most stable CO adsorption geometries (on *F* sites and on *D* sites) to the best C/O coadsorption structures (Fig. 7) were mapped out with the CI-NEB method. Several minimum energy paths (MEPs) were calculated and the barriers obtained vary between 0.77 eV and 3.27 eV. Here we focus on the two lowest barrier paths, $CO_G \rightarrow C/O_{C\_O\_2}$ (barrier 0.99 eV, shown in Fig. 9) and $CO_G \rightarrow C/O_{C\_O\_4}$ (barrier 0.77 eV, shown in Fig. 10). The path $CO_G \rightarrow C/O_{C\_O\_2}$ is thermodynamically the most favored one of the studied paths. This reaction is exothermic by 0.69 eV. In the transition state, the C–O bond is elongated to 1.25 Å, with the O atom close to a bridge site (Fig. 9). This type of transition state is quite common for CO dissociation on transition metal surfaces [44, 45, 48]. In the final structure, the C atom becomes embedded into the cluster surface, whereas the O atom is on the surface. Although the path $CO_G \rightarrow C/O_{C\_O\_2}$ has the largest ΔE, the $CO_G \rightarrow C/O_{C\_O\_2}$ path is kinetically the most favored one. This reaction is exothermic by 0.16 eV. The CO first moves to the edge of the face, reorients itself, and then goes through a transition state where CO tilts on the vertex of the cluster. Early temperature-programmed desorption (TPD) and time-resolved electron energy loss spectroscopy (TREELS) studies conducted by Whitman et al. [50] determined

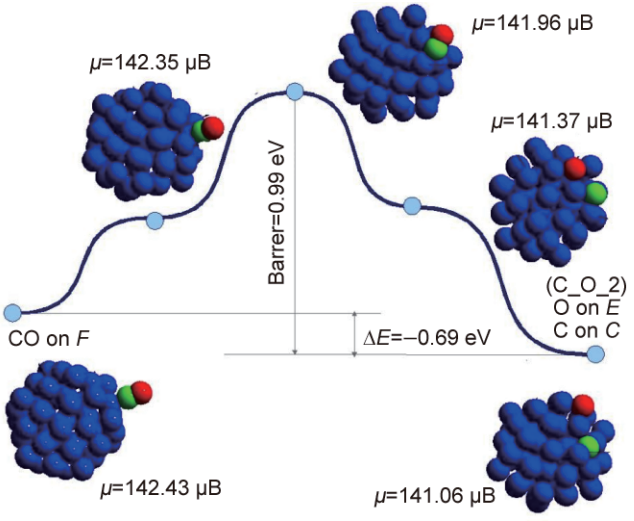

Figure 9 Calculated minimum energy paths for CO dissociation on a facet of Fe_{55}. Several intermediate structures along the path are shown (Fe, blue; C, green; and O, red)

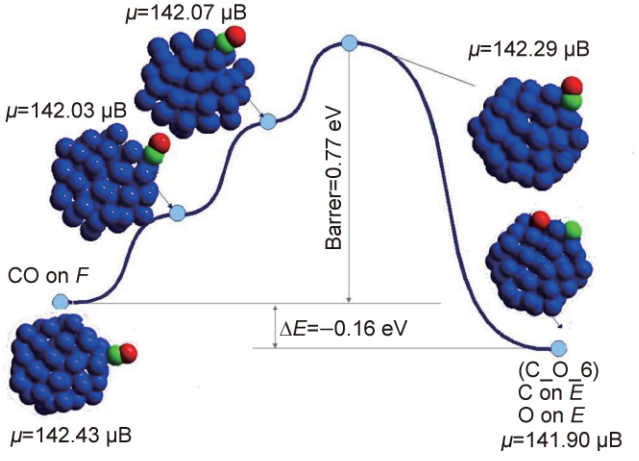

Figure 10 Calculated minimum energy paths for CO dissociation on a step of Fe_{55}. Several intermediate structures along the path are shown (Fe, blue; C, green; and O, red)

the kinetic data for CO adsorption and reaction on Fe(111). It was observed that at a monolayer coverage of 0.312, in addition to dissociation, some of the adsorbed CO desorbs with a barrier of ~1.4 eV. This can be taken as the upper limit for the CO dissociation barrier on this surface. If the predicted minimum MEPs for CO dissociation are compared with those from calculations for other surfaces, it can be seen that the paths are similar and but the presence of the vertex lowers the barrier of the dissociation reaction. The activation barrier of 0.77 eV obtained during our calculation is significantly lower than most of the reported barriers for different

surfaces (even the lowest case, 0.78 eV [46], is very close to that in our calculations), suggesting that the Fe_{55} is much more reactive towards CO dissociation than most of the stepped Fe surfaces. It seems that the ability of the metal atoms to activate reactants changes substantially as their coordination number is reduced, both at the atomic steps and the vertexes. The results show that the catalytically most active sites are the vertexes where the molecules also have a relatively low coordination number.

We consider a mechanism for the CO oxidation during the CVD synthesis that involves the reaction of the molecule with an oxygen atom adsorbed on the surface. In order to study the formation of CO_2 from CO and its fragment adsorbed on the cluster, the CO/O/C and CO_2/C co-adsorption geometries have been studied. The most stable geometries are indicated in Figs. 11 and 12, respectively. Taking CO_C_O_1 (Fig. 11) as the starting point, possible paths to CO_2_C_1 (Fig. 12) can be easily conceived. The corresponding structures of all transition states and intermediates are depicted in Fig. 13 together with the energy profile. The formation energy obtained is –0.37 eV, with a barrier of 1.13 eV. This path presents an elementary rearrangement of atoms and molecules on the surface. A more complex reaction path was found taking CO_C_O_2 (Fig. 11) as the starting point and CO_2_C_2 (Fig. 12) as the final point of the path. This path has a formation energy of +0.88 eV and barrier of 1.08 eV. Considering that the particle morphology and the reaction conditions are different, the calculated data are in reasonable agreement with

Adsorbate	Adsorption site Label	CO molecule	C atom	O atom	ΔE (eV/CO molecule)	μ (μB)	Geometry
CO (molecule) + O (atom) + C (atom)	CO_C_O_1	F	E	A	−0.78	139.10	
	CO_C_O_2	F	E	E	−1.80	139.44	

Figure 11 Stable geometries of CO + C + O on Fe_{55} (Fe, blue; C, green; and O, red)

Adsorbate	Adsorption site Label	CO_2 molecule	C atom	ΔE (eV/CO molecule)	μ (μB)	Geometry
CO_2 (molecule) + C (atom)	CO2_C_1	B	E	−0.97	140.55	
	CO2_C_2	F	E	−1.36	140.24	

Figure 12 Stable geometries of C + CO_2 on Fe_{55} (Fe, blue; C, green; and O, red)

the experimental results of Li et al. [26] The calculated barriers are, furthermore, in good agreement with the experimental results for the Fe_2O_3 catalysts used in modern industrial applications (~0.90 eV) [47].

We can also compare the calculated results with our experimental results. The DFT results above show that CO disproportionation on a nanosized iron cluster is a multistep process in which the rate limiting step is the formation of CO_2 from O and CO. We studied different reaction channels, and the lowest energy channel showed a barrier of 1.08 eV that is similar to the value obtained from the kinetic investigations, with a barrier of 0.65 eV for the overall process. The difference between the calculated and experimental results is reasonable and it can be justified considering that the cluster geometry and dynamics differ markedly in the two cases. The computed nanoparticle is very small and regular and thus it has few active sites. In this sense it is probably rather unreactive as a nanocluster. The larger clusters relevant to the experiments will have many more active sites and some of these can have lower activation barriers. Also, our calculations are at 0 K, so Fe atom diffusion is not taken into account, whereas the experiments are carried out around 900 K where the Fe atoms are very mobile. The iron mobility can also generate new active sites that are very difficult to model with static calculations. Even although the difference between the experimental and simulated clusters is rather large, we want to emphasize that the calculations have provided new information about the reactivity of nanoclusters and comparisons to real-world systems are more relevant at lower temperatures.

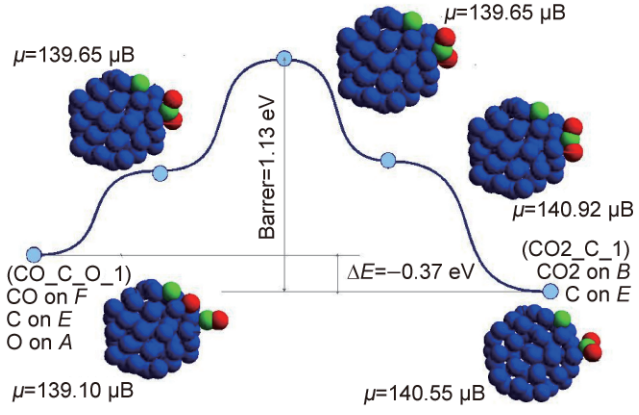

Figure 13 Calculated minimum energy paths for CO_2 formation on Fe_{55} starting from CO and co-adsorbed atomic C/O. Several intermediate structures along the path are shown (Fe, blue; C, green; and O, red)

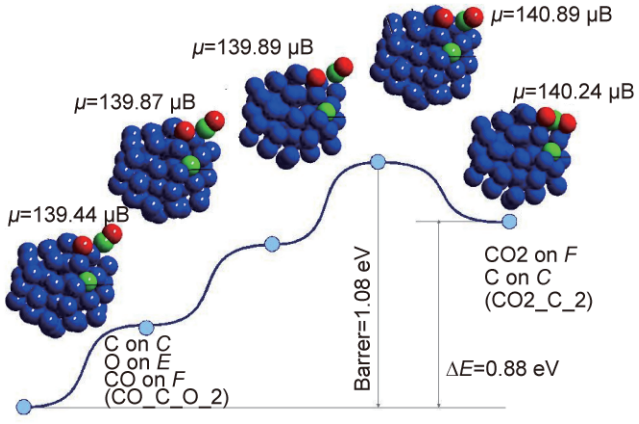

Figure 14 Calculated minimum energy paths for CO_2 formation on Fe_{55} starting from CO and co-adsorbed atomic C/O. Several intermediate structures along the path are shown (Fe, blue; C, green; and O, red)

3. Conclusions

We have presented an *ab initio* study of CO adsorption and dissociation, H_2 dissociation, and CO_2 formation on a small iron nanoparticle. To our knowledge, this is the first computational study of a chemical reaction on a real nanosized iron particle. Even more importantly, we have studied active sites that have not been studied before, the facets and vertexes. Overall, we see the small clusters as new and important model systems for nanocatalyst studies. They exhibit new active sites that complement those on stepped surfaces studied in other calculations. When the computational capacity permits, larger clusters can also be studied. At present, detailed chemical reactions can be studied for clusters with a size of 50–100 atoms. Another novel aspect of our study is the use of spin polarization with non-collinear magnetic moments.

In our calculations, the Fe_{55} cluster is found to have high catalytic activity. We have observed one important effect: the increased reactivity of low coordinated molecules on the vertexes. Such sites are particularly abundant on small nanosized particles, and they very likely explain their catalytic activity. We have been able to show that the reaction barriers for both CO dissociation and CO_2 formation are relatively low and an exothermic path for surface bound elemental carbon has been found. Carbon atom formation is the initial step in CNT formation. Under CVD conditions, 1.5–2.5 nm sized clusters are the CNT catalysts. These clusters probably have a similar geometry to what we have studied here, and we believe that in this case the vertexes are also the catalytically active sites.

In this work, we have studied the carbon disproportionation reactions of CO and H_2 dissociation. In further studies, we will focus on subsurface carbon, carbon–carbon, hydrogen–oxygen and hydrogen–carbon reactions on the nanoparticle. These studies will give information about carbide formation and the possible role of hydrogen. We see that it is very challenging to study the full process of CNT formation with *ab initio* methods. Thus, less detailed methods, like tight-binding, could also be used, but for some of the early reaction steps the *ab initio* calculations can give very reliable information. Also such calculations will be an excellent reference for the less detailed calculations.

Acknowledgements

The authors would like to express their sincere thanks to Dr. A. S. Foster and Dr. A. V. Krasheninnikov for useful discussions. This project mainly used the existing computational facilities available at CSC (Center for Scientific Computing), Espoo. This work has been supported in part by the European Commission under the 6th Framework Programme (STREP project BNC Tubes, contract number NMP4-CT-2006-03350) and the Academy of Finland (project number 128445).

References

[1] Saito, R.; Dresselhaus, G.; Dresselhaus, M. S. *Physical Properties of Carbon Nanotubes*; Imperial College Press: London, 1998.

[2] Endo, M. Grow carbon fibers in the vapor phase. *Chemtech* **1988**, *18*, 568–576.

[3] Ebbesen, T. W.; Ajayan, P. M. Large-scale synthesis of carbon nanotubes. *Nature* **1992**, *358*, 220–222.

[4] Guo, T.; Nikolaev, P.; Rinzer, A. G.; Tomanek, D.; Colberg, D. T.; Smalley, R. E. Self-assembly of tubular fullerenes. *J. Phys. Chem.* **1995**, *99*, 10694–10697.

[5] Nikolaev, P.; Bronikowski, M. J.; Bradley, R. K.; Rohmund, F.; Colbert, D. T.; A. Smith, K.; Smalley, R. E. Gas-phase catalytic growth of single-walled C carbon nanotubes from carbon monoxide. *Chem. Phys. Lett*. **1999**, *313*, 91–97.

[6] Harutyunyan, A.; Pradhan, B.; Kim, U.; Chen, G.; Eklund, P. CVD synthesis of single wall carbon nanotubes under "soft" conditions. *Nano Lett*. **2002**, *2*, 525–530.

[7] Hata, K.; Futaba, D. N.; Minuzo, K.; Namai, T.; Yumura, M.; Ijima, S. Water-assisted highly efficient synthesis of impurity-free single-walled carbon nanotubes. *Science* **2004**, *306*, 1362–1364.

[8] Singh, C.; Shaer, M. S. P.; Koziol, K. K. K.; Kinloch, I. A.; Windle, A. H. Towards the production of large-scale aligned carbon nanotubes. *Chem. Phys. Lett*. **2003**, *372*, 860–865.

[9] Moisala, A.; Nasibulin, A. G.; Brown, D. P.; Jiang, H.; Khriachtchev, L.; Kauppinen, E. I. Single-walled carbon nanotube synthesis using ferrocene and iron pentacarbonyl in a laminar flow reactor. *Chem. Eng. Sci*. **2006**, *61*, 4393–4402.

[10] Baughman, R. H.; Zakhidov, A. A.; de Heer, W. A.; Carbon nanotubes—The route toward applications. *Science* **2002**, *297*, 787–792.

[11] Ziolo, R. F.; Giannelis, E. P; Weinstein, B. A.; O'Horo, M. P.; Ganguly, B. N.; Mehrotra, V.; Russell, M. W.; Huffman, D. R. Matrix-mediated synthesis of nanocrystalline γ-Fe_2O_3: A new optically transparent magnetic material. *Science* **1992**, *257*, 219–223.

[12] Simon, U.; Schön, G.; Schmid, G. The application of Au_{55} clusters as quantum dots. *Angew. Chem. Int. Ed. Engl*. **1993**, *32*, 250–254.

[13] Yu, W.; Liu, H.; Tao, Q.; Modification of metal cations to metal clusters in liquid medium. *Chem. Commun*. **1996**, 1773–1774.

[14] Molina, L. M.; Hammer, B. Active role of oxide support during CO oxidation at Au/MgO. *Phys. Rev. Lett*. **2003**, *90*, 206102.

[15] Falsig, H.; Hvolbæk, B.; Kristensen, I. S.; Jiang, T.; Bligaard, T.; Christensen, C. H.; NØrskov J. K. Trends in the catalytic CO oxidation activity of nanoparticles. *Angew. Chem. Int. Ed. Engl*. **2008**, *47*, 4835–4839.

[16] Turner, M.; Golovko, V. B.; Vaughan, O. P. H.; Abdulkin, P.; Berenguer-Murcia, A.; Tikhov, M. S.; Johnson, B. F. G.; Lambert, R. M. Selective oxidation with dioxygen by gold nanoparticle catalysts derived from 55-atom clusters. *Nature* **2008**, *454*, 981–983.

[17] Campbell, C. T. The active site in nanoparticle gold catalysis. *Science* **2004**, *306*, 234–235.

[18] Kojima, I.; Kurahashi, M. Scanning tunneling microscope and atomic force microscope study of epitaxially grown palladium crystallites on graphite. *J. Vac. Sci. Technol.* **1994**, *B12*, 1780–1782.

[19] Ogura, S.; Sato, K.; Inoue, Y. E. Effects of RuO dispersion on photocatalytic activity for water decomposition of $BaTi_4O_9$ with a pentagonal prism tunnel and $K_2Ti_4O_9$ with a zigzag layer structure. *Phys. Chem. Chem. Phys*. **2000**, *2*, 2449–2454.

[20] Teramura, K.; Maeda, K.; Saito, T.; Takata, T.; Saito, N.; Inoue, Y.; Domen, K. Characterization of ruthenium oxide nanocluster as a cocatalyst with $(Ga_{1-x}Zn_x)(N_{1-x}O_x)$ for photocatalytic overall water splitting. *J. Phys. Chem. B* **2005**, *109*, 21915–21921.

[21] Nasibulin, A. G.; Moisala, A.; Brown, D. P.; Kauppinen, E. I. Carbon nanotubes and onions from carbon monoxide using $Ni(acac)_2$ and $Cu(acac)_2$ as catalyst precursors. *Carbon* **2003**, *41*, 2711–2724.

[22] Franklin, N. R.; Li, Y.; Chen, R. J.; Javey, A.; Dai. H. Patterned growth of single-walled carbon nanotubes on full 4-inch wafers. *Appl. Phys. Lett*. **2001**, *79*, 4571–4573.

[23] Jiang, H.; Nasibulin, A. G.; Brown, D. P.; Kauppinen, E. I. Unambiguous atomic structural determination of single-walled carbon nanotubes by electron diffraction. *Carbon* **2007**, *45*, 662–667.

[24] Nasibulin, A. G.; Brown, D. P.; Queipo, P.; Gonzalez, D.; Jiang, H.; Anisimov, A. S.; Kauppinen E. I. Effect of CO_2 and H_2 on the synthesis of single-walled CNTs. *Phys. Stat. Sol*. **2006**, *243*, 3087–3090.

[25] Kandalama, A. K.; Chatterjee, B.; Khanna, S. N.; Rao, B. K.; Jena, P.; Reddy, B. V. Oxidation of CO on Fe_2O_3 model surfaces. *Surf. Sci.* **2007**, *601*, 4873–4880.

[26] Li, P.; Miser, D. E.; Rabiei, S.; Yadav, R. T.; Hajaligo, M. R. The removal of carbon monoxide by iron oxide nanoparticles. *App. Catal. B: Env*. **2003**, *43*, 151–162.

[27] Kim, M. S.; Rodriguez, N. M.; Baker, R. T. K. The interaction of hydrocarbons with copper-nickel and nickel in the formation of carbon filaments. *J. Catal.* **1991**, *131*, 60–73.

[28] Reilly, P. T. A.; Whitten, W. B. The role of free radical condensates in the production of carbon nanotubes during the hydrocarbon CVD process. *Carbon* **2006**, *44*, 1653–1660.

[29] Raty, J. Y.; Gygi, F.; Galli, G. Growth of carbon nanotubes on metal nanoparticles: A microscopic mechanism from *ab initio* molecular dynamics simulations. *Phys. Rev. Lett*. **2005**, *95*, 096103.

[30] Feng, D.; Bolton, K.; Rosén, A. Molecular dynamics study of SWNT growth on catalyst particles without temperature gradients. *Comp. Mater. Sci*. **2006**, *35*, 243–246.

[31] Nasibulin, A. G.; Queipo, P.; Shandakov, S. D.; Brown, D. P.; Jiang, H.; Pikhitsa, P. V.; Tolochko, O. V.; Kauppinen. E. I. Studies on mechanism of single-walled carbon nanotube formation. *J. Nanosci. Nanotechnol*. **2006**, *6*, 1233–1246.

[32] Nasibulin, A. G.; Moisala, A.; Brown, D. P.; Jiang, H.; Kauppinen, E. I. A novel aerosol method for single walled carbon nanotube synthesis. *Chem. Phys. Lett*. **2005**, *402*, 227–232.

[33] Kresse, G.; Hafner, J. Norm-conserving and ultrasoft pseudopotentials for first row and transition elements. *J. Phys. Condens. Matter*. **1994**, *6*, 8245–8257.

[34] Kohler, C.; Seifert, G.; Frauenheim, T. Magnetism and the potential energy hypersurfaces of Fe_{53} to Fe_{57}. *Comp. Mater. Sci*. **2006**, *35*, 297–301.

[35] Chen, Y. H.; Cao, D. B.; Yang, J.; Li, Y. W.; Wang, J. G.; Jiao, H. Density functional theory study of CO adsorption on the Fe (111) surface. *Chem. Phys. Lett*. **2004**, *400*, 35–41.

[36] Sun, X.; Förster, S.; Li, Q. X.; Kurahashi, M.; Suzuki, T.; Zhang, J. W.; Yamauchi, Y.; Baum, G.; Steidl, H. Spin-polarization study of CO molecules adsorbed on Fe (110) using metastable-atom deexcitation spectroscopy and first-principles calculations. *Phys. Rev. B* **2007**, *75*, 035419.

[37] Freund, H. J.; Roberts, M. W. Surface chemistry of carbon dioxide. *Surf. Sci. Rep*. **1996**, *25*, 225–273.

[38] Henkelman, G.; Jonsson, H. Improved tangent estimate in the NEB method for finding minimum energy paths and saddle points. *J. Chem. Phys*. **2000**, *113*, 9978–9985.

[39] Henkelman, G.; Uberuaga, B. P.; Jonsson, H. A climbing-image NEB method for finding saddle points and minimum energy paths. *J. Chem. Phys.* **2000**, *113*, 9901–9904.

[40] Jiang, D. E.; Carter, E. A. Carbon atom adsorption and diffusion into Fe (110) and Fe (100) from first principle. *Phys. Rev. B* **2005**, *71*, 045402.

[41] Huo, C. F.; Ren, J.; Li, Y. W.; Wang, J.; Jiao, H. CO dissociation on clean and hydrogen precovered Fe (111) surfaces. *J. Catal*. **2007**, *249*, 174–184.

[42] Liao, X. Y.; Cao, D. B.; Wang, S. G.; Ma, Z. Y.; Li, Y. W.; Wang, J. G.; Jiao, H. J. Density functional study of CO adsorption on the (100), (001), and (010) surface of Fe_3C. *J. Mol. Catal. A: Chem.* **2007**, *269*, 169–178.

[43] Nasibulin, A. G.; Pikhitsa, P. V.; Jiang, H.; Kauppinen, E. I. Correlation between catalyst particle and single-walled carbon nanotube diameters. *Carbon* **2005**, *43*, 2251–2257.

[44] Jiang, D. E.; Carter, E. A. Adsorption and dissociation of CO on Fe (110) from first principle. *Surf. Sci*. **2004**, *570*, 167–177.

[45] Sorescu, D. C.; Thompson, D. L.; Hurley, M. M.; Chabalowski, C. F. First-principles calculations of the adsorption, diffusion, and dissociation of a CO molecule on the Fe (100) surface. *Phys. Rev. B* **2002**, *66*, 035416.

[46] Borthwick, D.; Fiorin, V.; Jenkins, S. J.; King, D. A. Facile dissociation of CO on Fe (211): Evidence from microcalorimetry and first-principles theory. *Surf. Sci.* **2008**, *602*, 2325–2332.

[47] Colonna, S.; De Rossi, S.; Faticanti, M.; Pettiti, I.; Porta, P. XAS characterization and CO oxidation on zirconia-supported $LaFeO_3$ perovskite. *J. Mol. Catal. A: Chem.* **2002**, *187*, 269–276.

[48] Liu, Z. P.; Hu, P. An insight into alkali promotion: A density functional theory study of CO dissociation on K/Rh (111). *J. Am. Chem. Soc.* **2001**, *123*, 12596–12604.

[49] Watanabe, M.; Kadowaki, T. Dissociation reactions of CO Gas on Fe and Fe_3O_4 surfaces observed by Raman-ellipsometry spectroscopy. *Appl. Surf. Sci*. **1987**, *28*, 147–166.

[50] Whitman, L. J.; Richter, L. J.; Gurney, B. A.; Villarrubia, J. S.; Ho, W. Coadsorption site occupation on Fe (111) vs coverage and temperature: The kinetics of adsorption and reaction. *J. Chem. Phys.* **1989**, *90*, 2050–2062.